The Astrophysical Journal, 622:116–128, 2005 March 20

THE *B*-BAND LUMINOSITY FUNCTION OF RED AND BLUE GALAXIES UP TO $z = 3.5$

E. Giallongo,[1] S. Salimbeni,[1] N. Menci,[1] G. Zamorani,[2] A. Fontana,[1] M. Dickinson,[3]
S. Cristiani,[4] and L. Pozzetti[2]

Received 2004 September 8; accepted 2004 November 30

ABSTRACT

We have explored the redshift evolution of the luminosity function of red and blue galaxies up to $z = 3.5$. This was possible by joining a deep *I*-band composite galaxy sample, which includes the spectroscopic K20 sample and the Hubble Deep Field samples, with the deep $H_{AB} = 26$ and $K_{AB} = 25$ samples derived from the deep NIR images of the Hubble Deep Field–North and Hubble Deep Field–South, respectively. About 30% of the sample has spectroscopic redshifts and the remaining fraction well-calibrated photometric redshifts. This allowed us to select and measure galaxies in the rest-frame blue magnitude up to $z \sim 3$ and derive the redshift evolution of the *B*-band luminosity function of galaxies separated by their rest-frame $U - V$ color or specific (i.e., per unit mass) star formation rate. The class separation was derived from passive evolutionary tracks or from their observed bimodal distributions. Both distributions appear bimodal at least up to $z \sim 2$, and the locus of red/early galaxies is clearly identified up to these high redshifts. Both luminosity and density evolutions are needed to describe the cosmological behavior of the red/early and blue/late populations. The density evolution is greater for the early population with a decrease by 1 order of magnitude at $z \sim 2-3$ with respect to the value at $z \sim 0.4$. The luminosity densities of the early- and late-type galaxies with $M_B < -20.6$ appear to have a bifurcation at $z > 1$. Indeed, while star-forming galaxies slightly increase or keep constant their luminosity density, "early" galaxies decrease in their luminosity density by a factor of $\sim$5–6 from $z \sim 0.4$ to $z \sim 2.5-3$. A comparison of one of the latest versions of the hierarchical cold dark matter models shows a broad agreement with the observed number and luminosity density evolutions of both populations.

Subject headings: galaxies: distances and redshifts — galaxies: evolution — galaxies: formation

1. INTRODUCTION

The redshift evolution of the galaxy luminosity function (LF) in different bands is a powerful probe of the main physical processes governing the assembly and subsequent activity of galaxies. In particular, the analysis of the LF of galaxies having different spectral and/or morphological properties can help to disentangle different histories of star formation.

In the emerging picture, galaxies form hierarchically through mergers of preexisting smaller galaxies in the context of the cold dark matter (CDM) scenario. In this picture early-type galaxies, which are generally among the brightest and massive galaxies in the universe, tend to be the result of relatively late assembly. This appears in contrast to the old age inferred from their red colors and from recent observations by Cimatti et al. (2004) and Glazebrook et al. (2004) showing the presence of some massive galaxies at high redshift.

For this reason it is very important to analyze the abundance as a function of redshift of early-type galaxies selected on the basis of their morphological appearance or spectral energy distributions (SEDs). This is a difficult task in both the observational and theoretical contexts: on the one hand we need large and deep surveys of NIR-selected galaxies to sample the rest-frame visual band up to at least $z \sim 3$; on the other hand, we need sophisticated Monte Carlo or hydrodynamical codes for galaxy formation and evolution in the CDM scenario.

Most of the information on the statistical analysis of the red/early or blue/late-type galaxies comes from local samples (e.g., Blanton et al. 2003; Baldry et al. 2004; Brinchmann et al. 2004). In these studies a clear bimodality appears in the color distribution of galaxies or their specific star formation rate (SSFR; i.e., per unit mass).

This bimodality separates the locus of the star-forming galaxies from the early population (early-type spirals, S0, and E0) and thus represents a useful tool to study the redshift evolution of galaxies having colors consistent with those of the early types independent of any morphological selection. In the local universe these different definitions appear to be consistent with each other (see, e.g., Schweitzer & Seitzer 1992).

In general, it is difficult to extract information about the star formation histories of individual early-type galaxies, since the stellar population evolving passively can become red in a much shorter time than the age of the galaxy. A complementary approach is given by the analysis of the redshift evolution of the LF of galaxies having different colors or SSFRs.

In this respect, recent attempts have been made in the local Sloan sample, for example, by Hogg et al. (2002), Blanton et al. (2003), and Baldry et al. (2004), and at intermediate redshifts by Bell et al. (2002). Preliminary results show that the rest-frame $U - V$ distribution of galaxies is bimodal up to $z \sim 1$ even for the field population. This allows a separation of the galaxy population in red/early and blue/late galaxies. In particular, the rest-frame *B*-band LF of the red galaxies shows a rather flat slope and evolves only mildly in qualitatively good agreement with the ΛCDM scenario.

An attempt to follow the evolution of galaxies of different spectral types at higher redshifts has shown, in particular, that the number density of early-type galaxies decreases with increasing redshift (Wolf et al. 2003). However, the authors used fixed SEDs to separate the galaxy spectral types, neglecting

[1] INAF, Osservatorio Astronomico di Roma, via Frascati 33, I-00040 Monteporzio, Italy.
[2] INAF, Osservatorio Astronomico di Bologna, via Ranzani 1, I-40127 Bologna, Italy.
[3] National Optical Astronomy Observatory, 950 North Cherry Street, Tucson, AZ 85719.
[4] INAF, Osservatorio Astronomico di Trieste, via G.B. Tiepolo 11, I-34131 Trieste, Italy.

evolutionary effects due to the passive stellar evolution with redshift. Moreover, the lack of NIR imaging in their sample has limited the analysis to $z \lesssim 1$.

The extension of this information at high redshifts indeed requires deep NIR surveys to get an estimate of the rest-frame $U - V$ color. The *J*- and *H*-band images in the Hubble Deep Field–North (HDF-N) and the *J*- and *K*-band images in the Hubble Deep Field–South (HDF-S) are among the deepest NIR images present in fields in which extensive multicolor optical imaging is already available and has been used to derive accurate photometric redshifts (Dickinson et al. 2003; Labbé et al. 2003; Fontana et al. 2003b; Poli et al. 2003, hereafter Paper I).

In this context, we have already used in Paper I a composite sample of NIR-selected galaxies that, although relatively small, has unique characteristics in many respects. It is a complete sample selected in the rest-frame *B* band from low to high redshifts, thanks to the deep NIR HDF-S images. It includes the area of the K20 survey (Cimatti et al. 2002) with a large fraction of spectroscopic redshifts at the bright end and well-tested photometric redshifts at the faint end. This composite sample has been used to derive the evolution of the global rest-frame *B*-band LF up to $z \sim 3$. The main result was the presence of appreciable luminosity evolution of the bright end of the LF. Such a brightening could be produced by enhanced star formation at high redshifts, triggered by galaxy encounters in a CDM scenario (see Menci et al. 2004; Nagamine et al. 2004). This kind of evolution is dominated by the star-forming population, which is abundant at high redshift.

On the other hand, we have also explored the evolution in mass of the sample, exploring in particular the evolution of the mass function up to intermediate redshifts and the mass density up to $z \sim 3$ (Fontana et al. 2003b, 2004). This approach allowed us to follow the cosmological evolution of galaxies in a way that was less biased by episodes of starburst activity. At $z \lesssim 1$ little evolution is observed in the galaxy mass function derived from the K20 sample, while at higher redshifts a more pronounced decrease in the stellar mass density was found in the HDF-S up to $z \sim 3$, in broad agreement with ΛCDM models (see also Rudnick et al. 2003). However, the derived fraction of mass density with respect to the local value at these high redshifts shows field-to-field variations of about a factor of 2 if we compare the results obtained in the HDF-S field with those found by Dickinson et al. (2003) in the HDF-N.

To explore how different the star formation history can be in different galaxy populations, we derive in this paper the number and luminosity density evolutions of the galaxies as a function of their color or SSFR (i.e., per unit stellar mass) up to $z \sim 3$, and we compare the density evolution of the red/early or blue/late populations with that predicted by a Monte Carlo rendition of the Menci et al. (2004) ΛCDM model. In this paper all the magnitudes are in the AB system, and an $\Omega_\Lambda = 0.7$, $\Omega_M = 0.3$, and $H_0 = 70$ km s^{-1} Mpc^{-1} cosmology is adopted.

2. THE GALAXY SAMPLE

Our composite sample of galaxies covers, with similar depth, a range spanning from the UV down to the optical/NIR wavelengths and is described in detail in Paper I. Here we summarize its general characteristics and main improvements. The galaxies are selected in the I or NIR J, K bands depending on the redshift interval as explained below. A first photometric catalog has been derived combining the optical images in the HDF-S (Casertano et al. 2000) with the deep ESO VLT NIR images obtained in the framework of the FIRES project (Labbé et al. 2003). Our infrared catalog reaches formal 5 σ limits in an aperture of 1.″2 at $J_{\rm AB} = 25.3$, $H_{\rm AB} = 24$, and $K_{\rm AB} = 25$. In the I band the HDF-S galaxies have been selected down to $I_{\rm AB} = 26.2$. In the HDF-N we used the same $K_{\rm AB} < 23.5$ catalog as that in Paper I. In addition to the sample used in Paper I, we adopted the HDF-N multicolor catalog of galaxies selected in the NICMOS H band by Dickinson et al. (2000), which is highly (>95%) complete down to $H_{\rm AB} < 26$ or $I_{\rm AB} < 25.8$, where the relatively bright limit in the I band was required to ensure detection in the NIR bands. We also used a brighter sample of galaxies selected in two fields centered around the QSO 0055−269 and in the *Chandra* Deep Field–South (Giacconi et al. 2001) for a total of $\simeq 68$ arcmin^2. This sample was used to select the targets for the so-called K20 ($K_{\rm AB} \leq 21.9$) spectroscopic survey (Cimatti et al. 2002). The catalogs in the latter two fields have been used to derive complete (>95%) samples down to $I_{\rm AB} = 24.5$ and 25, respectively. Detection in the NIR bands is ensured for all the galaxies in the composite sample.

To obtain the total fluxes of the objects in the chosen reference band, SExtractor Kron magnitudes (Bertin & Arnouts 1996) have been adopted for bright sources. For faint sources in ground-based images, we estimated aperture magnitudes with aperture corrections computed by estimating the flux losses outside the adopted aperture with respect to the Kron magnitudes for relatively bright sources. The reliability of the adopted correction has been tested by means of simulations as performed in Paper I and Poli et al. (2001). No appreciable systematic losses of the total flux for the faintest sources were found in addition to the well-known losses of 5%–10% typical of the Kron magnitudes. Moreover, Bouwens et al. (2004) have recently compared images obtained by the *Hubble Space Telescope* Advanced Camera for Surveys (ACS) in the Ultra Deep Field with those obtained in the same area from the shallower ACS-GOODS survey. The main result is that there are no specific biases due to surface brightness dimming in the evaluation of the typical galaxy sizes and, consequently, on the estimate of their total magnitudes up to high redshifts. To cope with the inhomogeneous quality of the different images, we produced a set of seeing-corrected *color* magnitudes that have been scaled to total magnitudes in all the bands (see, e.g., Vanzella et al. 2001). This ensures that colors used to estimate the redshifts are measured in the same physical region at all wavelengths, independently of the seeing FWHM present in each image. A fraction of 29% of the sample has spectroscopic redshifts, mainly from the K20 survey (Cimatti et al. 2002) and the spectroscopic follow-up in the GOODS/Chandra field (Vanzella et al. 2004) and the HDF-N (e.g., Cohen et al. 2000). For all the other galaxies, reliable photometric redshifts have been derived with a homogeneous technique, described in Fontana et al. (2000) and in Cimatti et al (2002). The model adopts several galaxy ages and exponentially declining star formation histories and includes Lyman absorption from the intergalactic medium and dust absorption with different amounts up to $E(B - V) = 1$, using both SMC and Calzetti extinction curves. In all the samples, the relative accuracy is $\sigma_{\Delta z} \lesssim 0.05$, where $\Delta z = (z_{\rm spe} - z_{\rm phot})/(1 + z_{\rm spe})$.

Our combined sample allows the computing of the 4400 Å rest-frame LF continuosly from $z \sim 0.4$ up to $z \sim 3.5$. The galaxy luminosity in this rest-frame wavelength is not strongly affected by dust, is directly observed up to high redshift in the NIR bands, and can easily be compared with local estimates of the blue LF. As in Paper I, we used our I-band selected sample for galaxies at $z < 1$. Indeed, the 4400 Å rest-frame wavelength is within or is shorter than the I band, and the LF includes all the galaxies with $m[4400(1 + z)] \leq I_{\rm AB}({\rm lim})$ of the various samples. This implies that some galaxies from the original $I_{\rm AB}$-limited

samples are excluded from the LF since they have a red spectrum, and consequently $m[4400(1+z)]$ are fainter than our adopted threshold. We have in this way extracted a complete subsample of galaxies having a continuum magnitude threshold at 4400 Å in each redshift interval, independent of their color [assuming galaxies in this redshift interval have $(R-I)_{\rm AB} \geq 0$]. The same procedure has been adopted at higher z using the K- or H-band selected sample. In the $1.3 < z < 2.5$ and $2.5 < z < 3.5$ intervals, the 4400 Å rest-frame wavelength is within or shorter than the H and K bands, respectively. The LF includes all the galaxies with $m[4400(1+z)] = m_{\rm AB} \leq m_{\rm AB}({\rm lim})$, where $m_{\rm AB} \equiv H_{\rm AB}$ or $K_{\rm AB}$ for $1.3 < z < 2.5$ and $m_{\rm AB} \equiv K_{\rm AB}$ for $2.5 < z < 3.5$. Finally, as in Paper I, the rest-frame absolute AB magnitude M_B(AB) has been derived from the theoretical best-fit SED for each galaxy. The same fit provides the photometric redshift for each galaxy. In this way the K-correction has been derived for each galaxy from the interpolation between the observed magnitudes using the best-fit spectrum. Uncertainties in this interpolation produce, on average, small ($\lesssim$10%) errors in the rest-frame luminosities (Ellis 1997; Pozzetti et al. 2003).

3. THE EVOLUTION AS A FUNCTION OF COLOR AND STAR FORMATION

To explore the evolution of the galaxy LF for different spectral types, we first analyzed the color distribution of galaxies as a function of redshift. In Figure 1 we show the distribution of the $U-V$ colors as a function of z for the two samples, the I band selected at $z < 1$, and the H and K bands selected at $z = 1.3-3.5$. The rest-frame $U-V$ color has been used because it includes the 4000 Å break, and thus it is most sensitive to the galaxy properties (age, star formation, etc.). Moreover, the $U-V$ color is always sampled by the multicolor catalog of our composite optical-NIR sample in a large-redshift interval up to $z \sim 3.5$. No correction for dust absorption has been applied to the rest-frame $U-V$ color.

Previous analyses of the LF evolution have adopted a constant rest-frame color to separate red/early-type galaxies from the blue/star-forming population (e.g., the Canada-France Redshift Survey sample; Lilly et al. 1995). However, when extending this criterion to high redshifts, we cannot ignore evolutionary effects in the stellar population of high-z galaxies. As a first attempt to include this effect, we assumed a scenario in which the star formation history of the red/early galaxy population is controlled by passive stellar evolution from a high formation redshift. Thus, we adopted the pure luminosity evolution (PLE) evolutionary color track of a galaxy whose local color is similar to the average color of a typical S0 galaxy as a criterion to separate the galaxy populations. In this way we can follow the blueing of the early-type population seen at increasing redshifts, assuming that only passive evolution was active in the past.

In Figure 1 the "S0 evolutionary track" is shown as a function of z. A formation redshift of $z = 10$, an exponential timescale $\tau = 3$ Gyr, and solar metallicity have been adopted to provide at $z = 0$ the typical color $U-V \sim 2.1 \pm 0.1$ of this class of galaxies (Schweizer & Seitzer 1992). The latest version of the standard Bruzual & Charlot (2003) model has been adopted. This evolutionary track naturally follows the evolution in redshift of the blue edge of the underdense regions occupied by red objects in the observed bimodal color distribution. The color separation increases as the redshift decreases from $U-V \sim 1$ at $z \sim 2.5$ to $U-V \sim 1.5$ at $z \sim 0.7$, as shown in Figure 1. Above the cut, the spread in the colors can be represented by passive evolution with short ($\tau = 0.3,\ 1,$ and 3 Gyr), exponential star formation timescales with a high formation redshift ($z = 10$).

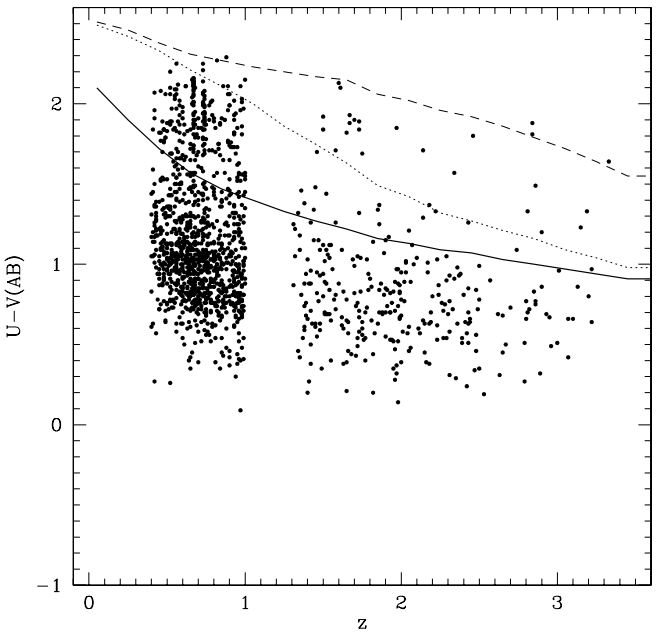

FIG. 1.—Rest-frame $U-V$ as a function of redshift. The continuous curve represents the color evolution due to the passive evolution of a galaxy formed at $z = 10$ and with a star formation timescale $\tau = 3$ Gyr. The Bruzual & Charlot (2003) code has been adopted. The resulting color at $z = 0$ is typical of an S0 galaxy. Dotted and dashed curves are derived adopting $\tau = 1$ and 0.3 Gyr, respectively, and could represent the reddest fraction of the sample.

Although the adopted evolutionary color cut is somewhat arbitrary, we have verified that small changes of the parameters do not significantly change the results and conclusions of the evolution of the red and blue populations outlined in § 5. The main constraint is that the evolutionary color tracks at $z \simeq 0$ should provide colors that are still consistent with those of S0 galaxies. There is room, for example, to reduce the formation redshift from $z = 10$ to 6. The new tracks would produce a blueshift of about 0.1 in the color cut at each redshift ($U-V \simeq 2$ at $z \simeq 0$). The resulting LF evolutions of the red and blue populations do not change appreciably, and the changes in the evolutionary parameters of the LFs are well within the errors.

It is clear, however, that if we are interested in the analysis of the galaxy evolution as a function of star formation activity, the use of a color criterion introduces some population mixing, since it is not possible to distinguish an early-type galaxy from a dusty starburst using only the $U-V$ color.

A further step in this direction can be obtained with a spectral fit to the overall SEDs by means of the Bruzual & Charlot (2003) spectral synthesis model. Although some degeneracy still remains, we can remove the most obvious starburst galaxies from the locus of early-type galaxies by considering the SSFR (i.e., per unit mass) $\dot{m}_*/m_*$ as a function of redshift that is plotted in Figure 2. The use of $\dot{m}_*/m_*$ in this context has a number of advantages with respect to using the SFR; for example, it is largely independent of cosmology, and it is less sensitive to the stellar initial mass function (IMF; see, e.g., Guzman et al. 1997; Brinchmann and Ellis 2000; Brinchmann et al. 2004). The library used to fit the galaxy properties (SFR and stellar mass) and derive photometric redshifts for the faint fraction of the sample is described in more detail in Paper I and Fontana et al. (2004). We are aware that the absolute values in the $\dot{m}_*/m_*$ distribution are subject to uncertainties due, for example, to the estimate of

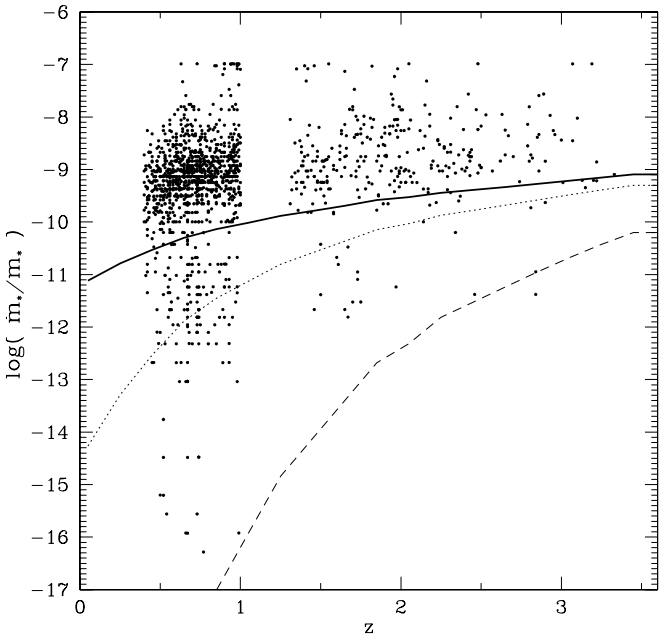

FIG. 2.—SSFR $\dot{m}/m$ as a function of redshift. The curves are obtained from the same models as in Fig. 1.

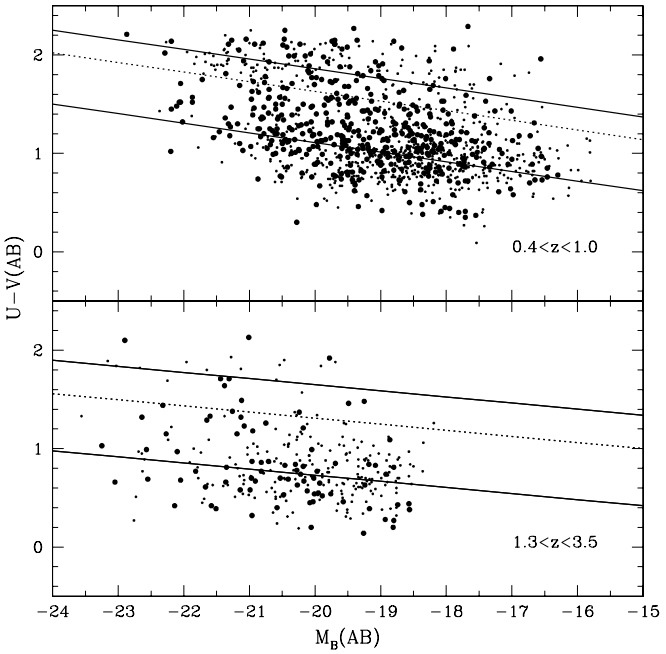

FIG. 3.—Color-magnitude relation in two redshift intervals. Black filled circles represent galaxies with $E(B-V) \geq 0.2$. Small dots represent galaxies with $E(B-V) < 0.2$. Thick lines represent the best-fit relations for the red and blue populations. Dotted lines represent the locus of the minimum between the two distributions used for the class separation.

the dust attenuation, which depends on the extinction curve adopted, and the methods adopted for the mass estimate. We refer in particular to the papers by Fontana et al. (2004) and Dickinson et al. (2003) for detailed description of the methods used to derive a reliable estimate of the stellar mass from the SED fitting procedure to our multicolor galaxy sample. We have recently quantified a systematic difference between the stellar mass derived from the best fit to the SED and that based on the so-called maximal age approach. The masses derived from the best-fit method are, in general, a factor of $\lesssim 2$ lower (Fontana et al. 2004). Any physical interpretation of the values produced in the observed $\dot{m}_*/m_*$ distribution should take into account all these uncertainties.

To explore how much the evolution of the red galaxies can be influenced by the presence of dusty starburst galaxies, especially at high z, we have separated the population according to the evolutionary track of the SSFR $\dot{m}_*/m_*$, which corresponds to the "S0 color track" already adopted. The evolution of the class separation appears evident in Figure 2. The evolutionary SSFR decreases from $\log(\dot{m}_*/m_*) \sim -9.4$ to $\log(\dot{m}_*/m_*) \sim -10.3$ (in units of yr^{-1}) from $z \sim 2.5$ to $z \sim 0.7$. Below the cut, the increasing spread in $\dot{m}_*/m_*$ with decreasing redshifts can be represented by passive evolution with short ($\tau = 0.3,\ 1,$ and 3 Gyr) exponential star formation timescales with a high formation redshift ($z = 10$).

The color/SSFR S0 evolutionary tracks will be used in § 5 to provide the separation of the galaxy populations at different redshifts and analyze their LF evolutions under the assumption that the star formation history of the red galaxies is mainly subject to stellar passive evolution.

4. THE BIMODAL COLOR/STAR FORMATION DISTRIBUTIONS AS A FUNCTION OF z

A different selection criterion, which is independent of the assumed evolutionary scenario, is based on the empirical analysis of the color or $\dot{m}_*/m_*$ distributions. Previous analyses at lower redshifts ($z < 1$) by Bell et al. (2004) and Baldry et al. (2004) have shown that these distributions are bimodal and thus identify two distinct populations, the red/early and blue/late galaxies. In the next section we analyze the color and SSFR distributions in our composite sample up to $z \sim 3$ to probe the presence of bimodality at high redshifts. The bimodality will be used as a further criterion to study the evolution of the LFs of the two populations.

4.1. *The Bimodal Color Distributions*

The inclusion of the deep HDF H- and K-band selected galaxies in our composite sample shows that this bimodality continues at least up to $z \sim 2-3$ and mainly separates blue/star-forming galaxies from the red/early-type population.

Previous analyses (e.g., Bell et al. 2004) have also shown that there is a weak luminosity dependence of the color separation induced by a color-magnitude relation. In Figure 3 this relation is shown for the two redshift intervals. To get a first evaluation of this relation we have simply fitted the distribution shown in Figure 3 with the sum of two Gaussians having the mean that is a linear function of the blue absolute magnitude. Each Gaussian has a constant dispersion, and each survey has been weighted with its covering sky area. Since the statistics of the red population are poor, we have adopted the same dependence on the absolute magnitude for both the blue and red populations. The maximum likelihood clearly identifies the locus of the blue population in the redshift interval $z = 0.4-1$, with a mean color that correlates with the absolute magnitude following the relation $\langle U-V \rangle = (-0.098 \pm 0.03)(M_B + 20) + (1.11 \pm 0.02)$ with a scatter $\sigma = 0.24$. For the red population we find $\langle U-V \rangle = (-0.098 \pm 0.03)(M_B + 20) + (1.86 \pm 0.03)$ with $\sigma = 0.24$.

In the magnitude range present in each redshift interval, the changes in the average colors of the two populations are, at most, $\Delta(U-V) \sim 0.3$ from $M_B = -17$ to -22. In the higher redshift interval $z = 1.3-3.5$ the statistics are poor, and the significance of the correlation is weaker. For the blue galaxies we derive

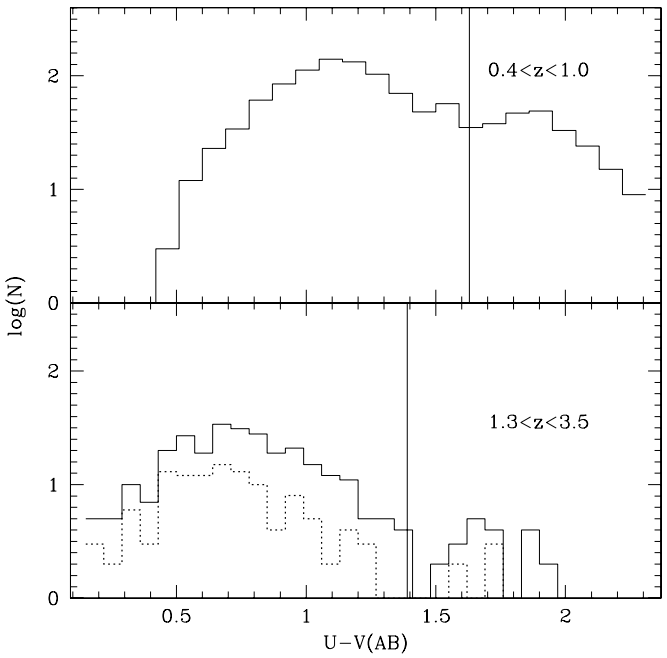

FIG. 4.—Color histograms in two redshift intervals. The continuous vertical lines represent the average separation evaluated from the color bimodal distribution. The lines are evaluated at the average redshift and at the average characteristic magnitude of the two Schechter populations ($M^* \simeq -19.9$ at $0.4 < z < 1$ and $M^* \simeq -21.2$ at $1.3 < z < 3.5$) for illustrative purposes. The dotted histogram represents the color distribution of galaxies in the redshift interval $2 < z < 3.5$.

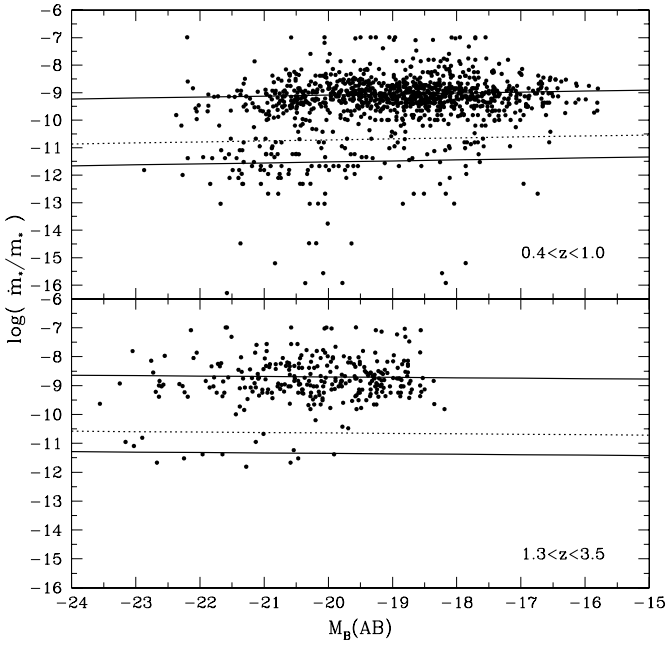

FIG. 5.—SSFR $\dot{m}/m$ as a function of M_B at different redshift intervals. Thick and dotted lines are the same as in Fig. 3.

$\langle U - V \rangle = (-0.062 \pm 0.017)(M_B + 20) + (0.73 \pm 0.01)$ with $\sigma = 0.25$, and for the red population $\langle U - V \rangle = (-0.062 \pm 0.017)(M_B + 20) + (1.65 \pm 0.28)$ with $\sigma = 0.42$. An intrinsic blueing as a function of redshift is apparent for both populations, as expected even in the case of pure passive evolution. At $M_B = -20$ from $z \sim 0.7$ to 2.5, it is $\Delta(U - V) \sim -0.4$ and -0.2 for the blue and red populations, respectively.

Taking into account the different normalizations of the two Gaussian distributions, it is possible at this point to find a formal minimum for the sum of the two distributions, which allows us to separate the blue from the red galaxy populations empirically. This locus is represented by the following color-magnitude relation $\langle U - V \rangle = -0.098(M_B + 20) + 1.64$ at $z = 0.4$–1 and $\langle U - V \rangle = -0.062(M_B + 20) + 1.31$ at $z = 1.3$–3.5 (Fig. 3, *dotted lines*). In the low-redshift bin our $U - V$ color separation is in good agreement with that found in the COMBO17 survey at $z \sim 0.5$ ($\langle U - V \rangle \sim 1.6$ at $M_B = -20$, after changing h and adopting an average $M_B - M_V = 0.5$ as derived from the red sample).

The histograms of the color distribution are shown in Figure 4 in the two redshift intervals. The histograms have been projected at the average characteristic magnitude of the two Schechter populations in the two redshift intervals for illustrative purpose. The vertical lines represent the average separation between the two populations evaluated from the color bimodal distribution.

We note in this context that the high-redshift interval in which the bimodal distribution is measured is rather large as required to keep sufficient statistics. Only a few red objects are indeed present in the sample at $z > 2$, and therefore we cannot firmly establish the presence of a bimodal distribution at these redshifts. However, the color distribution at $z > 2$ (Fig. 4, *dotted histogram*) is at least consistent with such a bimodality being already in place at $z > 2$.

4.2. *The Bimodal $\dot{m}_*/m_*$ Distributions*

Considering the corresponding $\dot{m}_*/m_*$ distributions, a bimodal shape appears at all redshifts, although its dependence on the rest-frame blue absolute magnitude is only marginally significant in the low-redshift bin and fully consistent with no correlation in the high-redshift bin (Fig. 5). Indeed, the same fitting procedure with two Gaussians gives $\langle \log \dot{m}_*/m_* \rangle = (0.036 \pm 0.016)(M_B + 20) - (9.09 \pm 0.03)$ for the "late" type galaxies and $\langle \log \dot{m}_*/m_* \rangle = (0.036 \pm 0.016)(M_B + 20) - (11.5 \pm 0.8)$ for the "early" population in the redshift interval $z = 0.4$–1. In the maximum likelihood analysis we have iteratively removed objects above 3 σ from the resulting Gaussian distributions. We also note that we call the two main populations of the bimodal distribution "late" and "early" without any specific reference to their morphological properties.

In the higher redshift interval $z = 1.3$–3.5 we obtain $\langle \log \dot{m}_*/m_* \rangle = (-0.015 \pm 0.040)(M_B + 20) - (8.7 \pm 0.1)$ for the late population and $\langle \log \dot{m}_*/m_* \rangle = (-0.015 \pm 0.040)(M_B + 20) - (11.4 \pm 0.2)$ for the early population. A small increase [$\Delta(\log \dot{m}_*/m_*) \sim 0.3,\ 0.1$] in the mean value of the SSFR with increasing redshift is apparent at $M_B = -20$ for both populations. This increase, of course, reflects the corresponding blueing of the two populations with increasing redshift, as recently observed, for example, by Rudnick et al. (2003) and Papovich et al. (2004). The errors in $\log \dot{m}_*/m_*$ derived from the spectral fit of each galaxy SED are of the same order ($\sim$0.15) for almost all the objects in the sample; therefore, error-weighted and unweighted ML analyses produce essentially the same result.

As in the case of the color distribution, it is possible to define a minimum between the two Gaussian distributions represented by the relation $\log \dot{m}_*/m_* = 0.036(M_B + 20) - 10.7$ at $z = 0.4$–1 and $\log \dot{m}_*/m_* = -0.015(M_B + 20) - 10.6$ at $z = 1.3$–3.5, weakly dependent on the absolute magnitude. The histograms of the SSFR distribution are shown in Figure 6 for the two redshift intervals, as in Figure 4 for illustrative purposes.

Thus, the much stronger and more significant color-magnitude correlation does not appear to be due mainly to appreciable changes of the SSFR with the rest-frame blue magnitude but

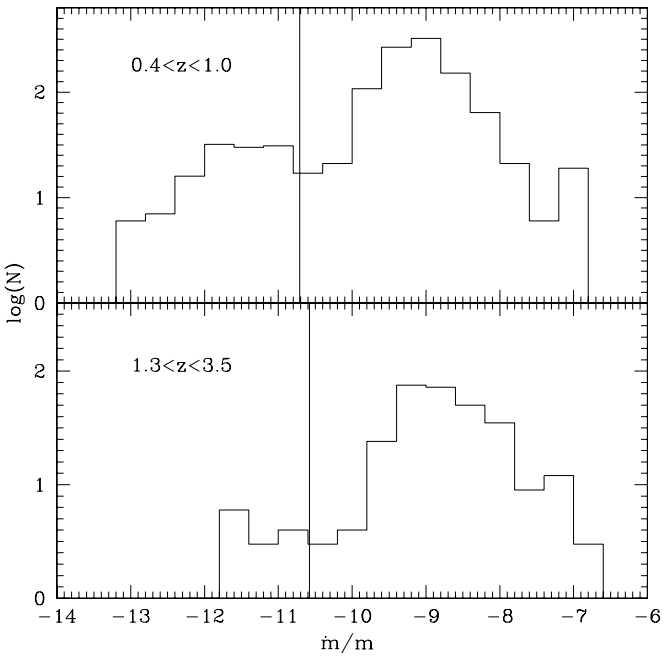

FIG. 6.—SSFR histograms. The continuous vertical lines represent the average separation evaluated from the SSFR bimodal distribution. The lines are evaluated at the average redshift and the average characteristic magnitude of the two Schechter populations ($M^* \simeq -19.7$ at $0.4 < z < 1$ and $M^* \simeq -21.2$ at $1.3 < z < 3.5$) for illustrative purposes.

more likely to variations of some other physical parameters. Keeping in mind the various degeneracies involved in the derivation of the galaxy physical parameters from the color fitting to the synthetic spectral models (see, e.g., Papovich et al. 2001; Fontana et al. 2004), it is interesting to note that the fitting analysis suggests dust reddening as the main reason for the observed color-magnitude correlation in the blue population. Indeed, the fraction of the blue galaxies with extinction $E(B-V) > 0.2$ (Fig. 3, *large symbols*) increases with the blue luminosity. In the redshift interval $z = 0.4-1$, considering the blue galaxies with colors within 2 σ of their average color-magnitude relation, the fraction of dusty galaxies is 36% and 60% for galaxies with $M_B > -20$ and $M_B < -20$, respectively. In the higher redshift interval $1.3 < z < 3.5$ the fraction increases from 24% at low luminosities to 40% at high luminosity, but the statistics is admittedly poor. This is in agreement with previous findings by Shapley et al. (2001) for the Lyman break galaxies at $z \sim 3$.

For the red population the change in the fraction of dusty galaxies from faint to bright galaxies is only 5%, and it is not sufficient to explain the observed color-magnitude correlation. However, the fraction of red galaxies with solar or greater than solar metallicity is higher (65%) for high-luminosity galaxies ($M_B < -20$) than for faint galaxies (50%) in agreement with what is found in the local early-type galaxy sample (see, e.g., Kuntschner et al. 2002). This last effect could more likely reproduce the observed correlation even at high redshift.

Although these results are dependent on several assumptions such as, for example, the adopted Salpeter IMF, they can help in identifying the main physical parameters that underlie the observed relations. Further analysis in this direction is outside the scope of this work.

Summarizing the analysis of this section, we have shown with this still limited sample that the bimodality in the distribution of the galaxy $U-V$ colors or SSFRs extends to high redshifts at least up to $z \sim 2$. A more robust statistical significance will be obtained with larger multicolor optical-NIR surveys.

Despite all the uncertainties, the derived bimodal distribution is clearly representative of the presence of two distinct populations, and it can be used to make an empirical separation of the galaxy populations at different redshifts to analyze their LF evolutions. This will be done in the next section.

5. THE EVOLUTION OF THE LUMINOSITY FUNCTIONS OF FIELD GALAXIES

5.1. *The Statistical Analysis*

The LF is computed extending the procedure used in Paper I. First of all, we have applied to our composite sample an extended version of the $1/V_{\max}$ algorithm as defined in Avni & Bahcall (1980) so that several samples can be combined in one calculation. Our combination of data from separate fields with different magnitude limits has been treated by computing for every single object a set of effective volumes, $V_{\max}(j)$, for each jth field under analysis. For a given redshift interval $(z_1,\ z_2)$, these volumes are constrained between z_1 and $z_{\rm up}(j)$, the latter being defined as the minimum between z_2 and the maximum redshift at which the object could have been observed within the magnitude limit of the jth field. The galaxy number density $\phi(M,\ z)$ in each $(\Delta z,\ \Delta M)$ bin can then be obtained as

$$\phi(M,\ z) = \frac{1}{\Delta M}\sum_{i=1}^{n}\left[\sum_{j}\omega(j)\int_{z_1}^{z_{\rm up}(i,j)}\frac{dV}{dz}\,dz\right]^{-1}, \quad (1)$$

where $\omega(j)$ is the area in units of steradians corresponding to the field j, n is the number of objects in the chosen bin, and dV/dz is the comoving volume element per steradian.

The Poisson error in each LF magnitude bin was computed adopting the recipe ofGehrels (1986), valid also for small numbers. The uncertainties in the LF due to the photometric z-estimates were computed as in Paper I, assuming the typical rms found comparing photometric and spectroscopic z. A set of 50 catalogs of random photometric z was produced using the above rms uncertainties to compute a set of 50 LFs. The derived fluctuations in each magnitude bin resulted in smaller than Poissonian errors and have been added in quadrature, although the errors are not independent among different bins and could be overestimated. Finally, in order to take into account (at least partially) the uncertainties due to the field-to-field variance, we have used the maximum between the Poisson error and the density variance among the fields in each bin of the LF. The resulting field-to-field variance is the main source of error in the LF bin.

The $1/V_{\max}$ estimator for the LF can be affected, in principle, by small-scale galaxy clustering, although in our case the large-redshift bins adopted would reduce the effect of any density fluctuation. For this reason a parametric maximum likelihood estimator is also adopted, which is known to be less biased with respect to small-scale clustering (see Heyl et al. 1997).

The parametric analysis of the galaxy LF has been obtained from the maximum likelihood analysis assuming a Schechter parametric form ϕ for the LF. The method used in Poli et al. (2003) and the present paper represents an extension of the standard Sandage et al. (1979) method, in which several samples can be jointly analyzed and the LF is allowed to vary with redshift. In the case of our composite survey, which is based on j-magnitude-limited fields, the maximum likelihood Λ has been

TABLE 1
Luminosity Function Parameters

Parameter	ϕ_0^*	M_0^*	α	δ	γ	N
Total	0.0056	-20.93 ± 0.23	-1.29 ± 0.04	1.48 ± 0.52	-0.65 ± 0.19	1434
$<U-V$ (S0).....	0.0042	-20.31 ± 0.26	-1.38 ± 0.05	2.35 ± 0.58	-0.52 ± 0.23	1142
$>U-V$ (S0).....	0.0106	-20.23 ± 0.28	-0.46 ± 0.10	2.72 ± 0.66	-2.23 ± 0.28	292
$>\dot{m}/m$ (S0)	0.0050	-20.55 ± 0.25	-1.33 ± 0.05	1.96 ± 0.56	-0.60 ± 0.22	1242
$<\dot{m}/m$ (S0).....	0.0044	-20.66 ± 0.36	-0.63 ± 0.11	2.08 ± 0.82	-1.80 ± 0.34	192

derived from the analysis of Marshall et al. (1983) after proper normalization of their probability function

$$\Lambda = \prod_{i=1}^{N} \frac{\phi(M_i,\ z_i)\, dz\, dM}{\sum_j \omega(j) \int_{z_1^j}^{z_2^j} (dV/dz) dz \int_{-\infty}^{M_{\rm lim}^j(z)} \phi(M,\ z)\, dM}, \quad (2)$$

where z_1 and z_2 are the minimum and maximum redshifts available for each sample, N is the total number of objects considered in the composite sample, and $M_{\rm lim}^j(z)$ is the corresponding absolute magnitude value at the given redshift z to the magnitude limit of the jth survey. The value of ϕ^* in Table 1 is then obtained simply by imposing a normalization on the best-fit LF such that the total number of galaxies of the combined sample is reproduced. A formal derivation of this equation can also be found in Heyl et al. (1997), where it is also shown that the present equation reduces to the standard Sandage et al. (1979) formulation in the case of a single survey and an LF that is constant in redshift.

At variance with Paper I, we allow the Schechter parameters ϕ^* and M^* to vary with redshift

$$\phi(M,\ z) = 0.4 \ln(10) \phi^*(z) [10^{0.4(M^*(z)-M)}]^{1+\alpha} \times \exp[-10^{0.4(M^*(z)-M)}],$$

where $\phi^* = \phi_0^*(1+z)^\gamma$ and $M^*(z) = M_0^* - \delta \log(1+z)$, equivalent in luminosity to $L^*(z) = L_0^*(1+z)^{0.4\delta}$. The slope α is kept constant with redshift, since it is well constrained only by the low-to-intermediate redshift data ($z < 1$).

We used the MINUIT package of the CERN library (James & Roos 1995) to minimize $-2 \ln \Lambda$. Since both the composite sample and the parametric analysis have been improved with respect to Paper I, we show in Figure 7 and the first row of Table 1 the results for the evolution of the LF of the overall sample. The errors in Table 1 correspond to errors for each interesting parameter, independently of the other parameters, obtained with a standard threshold of $2\Delta \ln \Lambda = 1$. A detailed analysis of the four-dimensional space is outside the scope of the present paper. However, if, for example, we consider the joint 68% confidence region for the M^*, α or γ, δ pairs of interesting parameters, we obtain after projection on the parameter axes individual errors that are about 1.6 times larger.

The inclusion of the deep NIR-selected HDF-N sample contributes to a better definition of the faint LF slope at intermediate redshifts ($z = 1.3-2.5$). As in Paper I, the local LFs from the Sloan (Blanton et al. 2001) and Two-Degree Field (2dF; Norberg et al. 2002) surveys have been included for comparison. The difference between the two local LFs shows the level of uncertainty present in the estimate of the LF even at about the same local redshift interval.

The evolution of the LF shown in Figure 7 by the $1/V_{\rm max}$ analysis shows little density evolution at the faint end with respect to the local values, while at the bright end a brightening by about 1 mag is apparent.

If we adopt a Schechter shape of the LF at all redshifts, the maximum likelihood analysis shows an average slope ($\alpha \simeq -1.3$) somewhat flatter than that found in Paper I. Moreover, appreciable density and luminosity evolution with redshift are needed to fit the data, as derived from the parameters in Table 1. We note in this respect that the magnitude limits of the samples cut the LF at progressively higher luminosities with increasing redshifts. For this reason we prefer to keep the α slope constant with redshift unless a bad agreement with the $1/V$max points is found. The mixed luminosity-density shift of the Schechter shape provides a LF that keeps an almost constant volume density with redshift at the faint end, while at the bright end it provides an appreciable luminosity evolution, in agreement with the qualitative results of the $1/V_{\rm max}$ analysis.

Figure 7 also shows the good agreement, better than the 2 σ level, between the parametric and the $1/V_{\rm max}$ LFs. This implies, in particular, that the assumed parametric evolutionary laws are an acceptable representation of the binned LF in the overall redshift interval. Moreover, the good agreement implies that any small-scale clustering does not appreciably affect the $1/V_{\rm max}$ estimate of the LF because of the large-redshift intervals adopted.

This kind of shape and evolution of the LF is the result of the different evolutions of distinct galaxy populations. For this reason we perform in the next section a separation of the galaxy

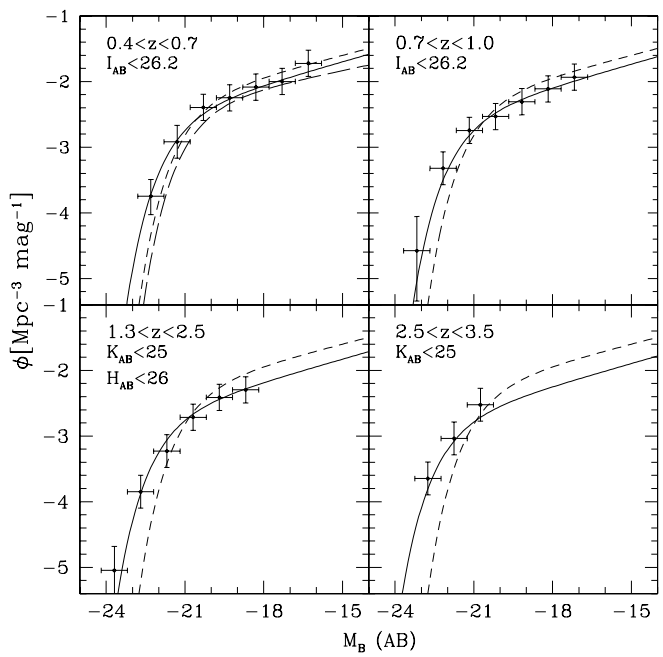

Fig. 7.—Total LF as a function of redshift. Continuous curves come from the maximum likelihood analysis. The local LFs from the Sloan and 2dF surveys are also shown as short and long-dashed curves, respectively, as in Paper I.

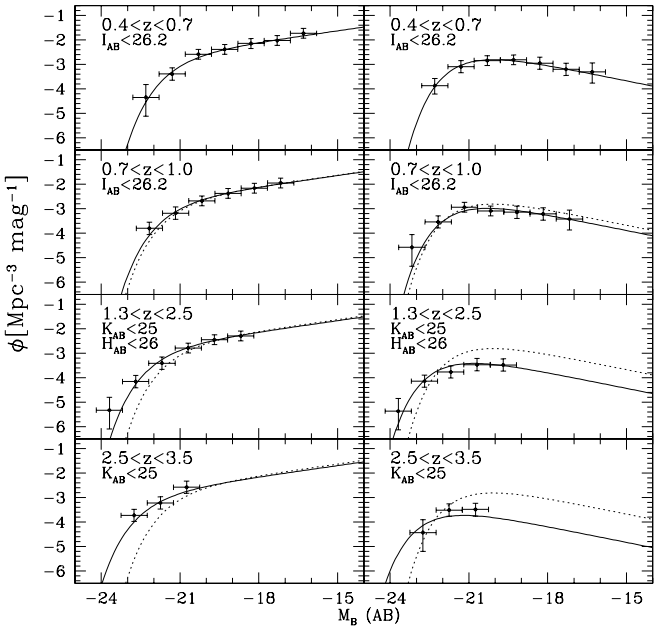

FIG. 8.—LF of blue (*left*) and red (*right*) galaxies separated in the rest-frame $U - V$ color following the S0 evolutionary track (see text for details). Continuous curves come from the maximum likelihood analysis. The LF in the lowest redshift bin $0.4 < z < 0.7$ is also shown for comparison in all panels (*dotted curve*).

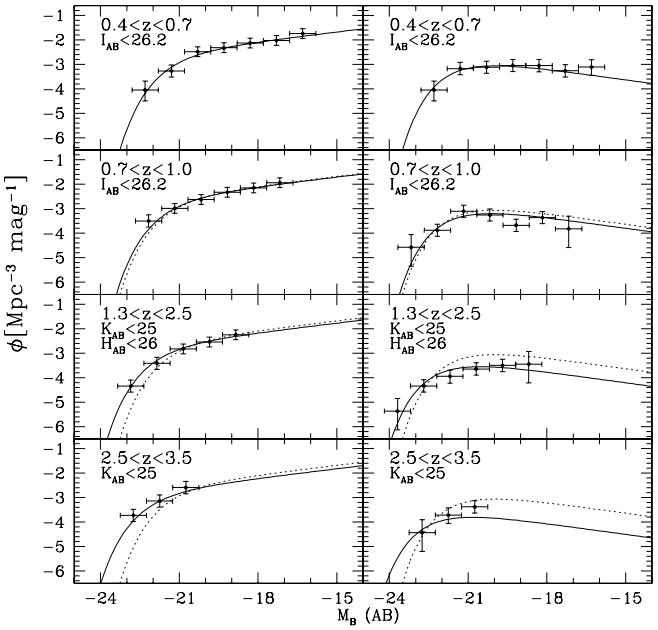

FIG. 9.—LF of late (*left*) and early (*right*) galaxies separated on the basis of their SSFR $\dot{m}_*/m_*$ following the S0 evolutionary track. The LF in the lowest redshift bin $0.4 < z < 0.7$ is also shown for comparison in all panels (*dotted curve*).

sample in the blue/late and red/early populations to probe the different evolutionary behavior of the two LFs.

5.2. *Passive Evolutionary Tracks as a Criterion to Separate Red/Early and Blue/Late Galaxies as a Function of z*

The LFs of the blue and red populations defined on the basis of the S0 color track are shown in Figure 8 in different redshift intervals. The parametric Schechter evolution has been derived adopting a mixed luminosity and density evolution with a constant slope. The model LF is shown at the average z of the bin for illustrative purpose.

The results of the maximum likelihood fits are shown in Table 1. Assuming the Schechter shape at all redshifts, we found that the average slope α of the two populations is clearly different, ranging from $\alpha \sim -1.3,\ -1.4$ for the blue/late galaxies to $\alpha \sim -0.5,\ -0.6$ for the red/early population. This result is already well known from previous works on the local and $z < 1$ samples (Lilly et al. 1995; Blanton et al. 2001; Bell et al. 2002). The shallower slope for the red/early sample implies that the ratio of the blue over the red population increases strongly to fainter magnitudes. The slope of the red LF is in particularly good agreement with the value of -0.6 ± 0.1 derived in the $z = 0-1$ interval by Bell et al. (2002) in their analysis of the wider but shallower COMBO17 survey. The δ and γ parameters of the luminosity and density evolution are significantly different from 0, suggesting that both evolutions are needed to provide a satisfactory fit. Both populations show comparable luminosity evolution, but the red population is characterized by a stronger density evolution with a decline of at least a factor of $\sim$5, from $z \sim 0.4$ to 3.

A comparison of the shape and evolution of the total LF computed in the previous section (see Table 1) shows that both the faint end slope and the amount of density evolution of the total LF are mainly driven by that of the blue population. To explore how much the evolution of the red galaxies can be influenced by the presence in this population of dusty starburst galaxies, especially at high z, we have separated the population according to the evolutionary S0 track of the SSFR $\dot{m}_*/m_*$.

The resulting LFs are similar to the previous ones with only mild differences (Fig. 9). From the last column of Table 1, in which the number of objects in each sample is given, it can be noted that about 35% of the red sample with colors redder than the S0 color track show an SED indicative of a dusty star-forming population. This fraction is similar to that found in spectroscopic surveys and does not alter the qualitative behavior about the LF evolutions.

It is clear that the presence of a mixed luminosity-density evolution in both populations implies, in particular for the red/early population, a star formation history more complex than that provided by the simple PLE model adopted here to separate the two populations, in which the burst of star formation is located at high redshifts ($z > 3$). This mixed evolution is directly seen in the $1/V_{\max}$ representation of the LFs in Figures 8 and 9, which shows that luminosity evolution is apparent mainly at the bright end of the LFs, while at the faint end the LFs appear affected by density evolution. This behavior will be discussed more quantitatively in § 6.

5.3. *The Empirical Bimodal Color and $\dot{m}_*/m_*$ Distributions as a Criterion to Separate Red/Early and Blue/Late Galaxies as a Function of z*

In the previous section we have shown that the evolutionary behavior of the red/early population does not follow that expected from PLE models, assuming a passive evolutionary scenario for the color or $\dot{m}_*/m_*$ separation. A selection criterion that is independent of the assumed evolutionary scenario is based on the empirical analysis of the color or $\dot{m}_*/m_*$ distributions as observed in our sample and already found at lower redshifts by Bell et al. (2002) and Baldry et al. (2004). In the previous section we have shown that these distributions are bimodal up to $z \lesssim 3$, and thus we identify two distinct populations. The peaks of the bimodal color distributions derived in the low- and high-redshift intervals are dependent on both

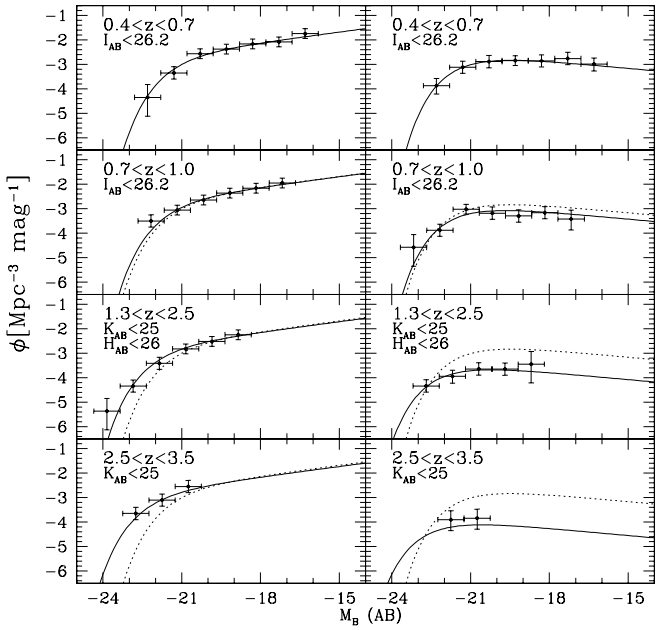

FIG. 10.—LF of late (*left*) and early (*right*) galaxies separated following their rest-frame $U - V$ colors as derived from the minimum in their bimodal Gaussian distributions. The LF in the lowest redshift bin $0.4 < z < 0.7$ is also shown for comparison in all panels (*dotted curve*).

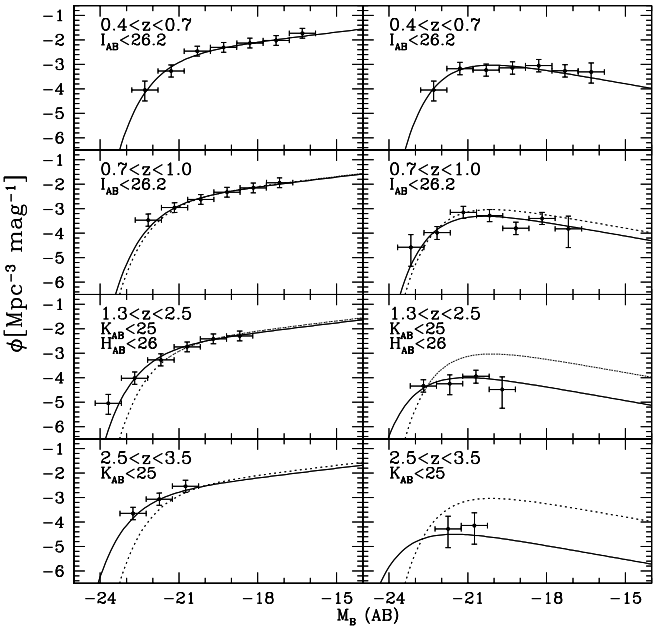

FIG. 11.—LF of late (*left*) and early (*right*) galaxies separated following their SSFR $\dot{m}_*/m_*$ as derived from the minimum in their bimodal Gaussian distributions. The LF in the lowest redshift bin $0.4 < z < 0.7$ is also shown for comparison in all panels (*dotted curve*).

redshift and luminosity, while the $\dot{m}_*/m_*$ distributions are less dependent on luminosity.

Using the locus of the minimum in the color and $\dot{m}_*/m_*$ distributions in the $0.4 < z < 1$ and $1.3 < z < 3.5$ intervals, we have derived the evolution of the LF of red/early and blue/late galaxies shown in Figures 10 and 11, whose parameters are shown in Table 2. In this case, in each of the two redshift intervals, the color separation is a function of the rest-frame blue absolute magnitude. At $M_B = -20$ the color that divides the two classes becomes redder by 0.3 mag from $z \sim 2.5$ to 0.7, similar to (albeit a bit smaller than) that predicted by the PLE color track used in the previous section.

For the red population we have compared our LF with that of Bell et al. (2002), finding a generally good agreement at relatively bright magnitudes and low redshifts. In particular, the slope of the red population is $\alpha = -0.76 \pm 0.10$, and even in this case it is in agreement with that found in the COMBO17 survey.

Although we do not consider the effects of uncertainties in the location of the minima of the bimodal distributions, we do not find a change in the qualitative evolutionary behavior of the two populations by comparing the LF results obtained using the S0 evolutionary track and the minima in the bimodal distributions. The main quantitative difference consists of a stronger density evolution (larger γ) for the red/early population in the bimodal case (since we are excluding some objects at high redshifts with respect to the "S0 cut").

Indeed, we can compare the LF of the early population selected to have $\log \dot{m}_*/m_* \lesssim -10.5, -10.6$ with the characteristic absolute magnitude $M^* = -21, -21.5$ (depending on redshift). At these magnitudes we are on the flat part of the LF, and thus we are less sensitive to changes in volume density due to any luminosity evolution. In Figure 11 we can see that the LF of the early sample declines by about 1 order of magnitude, from $z = 0.5$ to 3. This density evolution is somewhat smaller when considering the color-selected red sample because of the presence of some dusty starburst galaxies at high redshifts. Indeed, $\sim$40% of the red sample shows SEDs indicative of a dusty star-forming population.

6. NUMBER AND LUMINOSITY DENSITY EVOLUTIONS OF THE RED/EARLY AND BLUE/LATE GALAXIES

6.1. *Observed Behavior*

The values of the parameters of the mixed evolution we have derived for both populations are the result of the assumed parameterization of the LF with a Schechter function. To clarify the cosmological evolution of galaxies at different luminosities in a less model-dependent way, we evaluate directly the volume density of galaxies as a function of redshift in given bins of the rest-frame blue magnitude. We also evaluate the associated redshift evolution of the luminosity density observed in the rest-frame B band by the same galaxies. We show the results assuming both the S0 evolutionary track and the empirical separation derived from the bimodal distribution to separate the two populations.

Considering the former case, we note in Figure 12 that the cosmological evolution of the red/early galaxies appears to depend on their luminosity. Indeed, the faint galaxies, typically in the range $-21.5 < M_B < -20.6$ (where $M_B \simeq -20.6$ is at the faintest limit of the population at $z \sim 3$), decrease by a factor of $\sim$2–3 from $z \sim 0.5$ to 2.5. However, it is interesting to note that the brighter galaxies in the range $-23 < M_B < -22$ are consistent with being constant in the same redshift interval.

To allow a first simple quantitative comparison of a PLE scenario, we show in Figure 12 the expected evolution for galaxies with $-23 < M_B < -22$ obtained by adopting the local LF of red galaxies and evolving it in luminosity by adopting the S0 evolutionary track shown in Figure 1. The local value derived from the Sloan survey is included as derived from Bell et al. (2002). Although the COMBO17 sample has been derived from a slightly different color threshold, the intermediate-redshift values are in good agreement with our data.

The PLE behavior is similar to the observed evolution for $z < 1$, but it overestimates the data at high redshifts by a factor

TABLE 2
LUMINOSITY FUNCTION PARAMETERS

Parameter	ϕ_0^*	M_0^*	α	δ	γ	N
$<U-V$ (bimodal).....	0.0040	-20.47 ± 0.26	-1.36 ± 0.05	2.30 ± 0.57	-0.45 ± 0.22	1173
$>U-V$ (bimodal)	0.0110	-20.49 ± 0.38	-0.76 ± 0.10	2.70 ± 1.00	-3.10 ± 0.38	261
$>\dot{m}/m$ (bimodal).....	0.0050	-20.51 ± 0.24	-1.32 ± 0.05	2.15 ± 0.53	-0.56 ± 0.20	1282
$<\dot{m}/m$ (bimodal).....	0.0110	-20.23 ± 0.41	-0.53 ± 0.13	3.49 ± 1.01	-3.65 ± 0.47	152

of $\sim$5. This overestimate reduces to a factor of $\lesssim$3 if compared with the number density derived from the best-fit LFs. This would imply that dynamical events are important for the brightest red/early population at $z > 1$.

The *B*-band luminosity density derived from the same data is shown in Figure 13 and has the same behavior of the number density evolution. The data (*open circles*) represent the contribution from red/early galaxies with $M_B < -20.6$, which at $z \sim 3$ are at the faintest limit. In this way we can explore the evolutionary behavior over the entire redshift range of galaxies within the same luminosity range. At $z < 1$ we have also considered (*open triangles*) a lower limit $M_B < -19.5$ to compare the luminosity density at intermediate redshift with that of Bell et al. (2002), finding a broad consistency within the rather large errors. Our values, however, are about a factor of $\sim$2 higher, since the S0 track used to separate the two populations tends to include in the red population a higher number of galaxies with increasing redshifts with respect to the bimodal class separation used by Bell et al. (2002). The same PLE model is also shown in Figure 13, and the same discrepancy is apparent at $z > 1$.

Since the evolution is more complex than that expected from a PLE scenario, it is interesting to use the empirical criterion for the class separation based on the star formation bimodal distribution. The volume densities and the *B*-band luminosity densities of galaxies with $M_B < -20.6$ as a function of redshift are shown in Figure 14. In this case both the early and late populations are shown in each panel.

The cosmological evolutions of the bright late and early populations appear to have a bifurcation at $z > 1$. Indeed, while star-forming galaxies slightly increase or keep constant their number/luminosity density, early galaxies decrease in their number density by about 1 order of magnitude and in luminosity density by a significant factor of $\sim$5–6 (although with large statistical uncertainties), from $z \sim 0.4$ to $z \sim 2.5$–3. We have also plotted the luminosity density of both populations derived from the best-fit LFs extrapolated down to the minimum luminosity observed in our low-z LF, $M_B = -15.8$. The evolutionary trend is similar to that observed, albeit shifted in normalization by a factor of $\lesssim$2. It is important to note that the parametric representation used in this analysis is valid only in the adopted redshift interval $0.4 < z < 3.5$. Extending the analysis outside

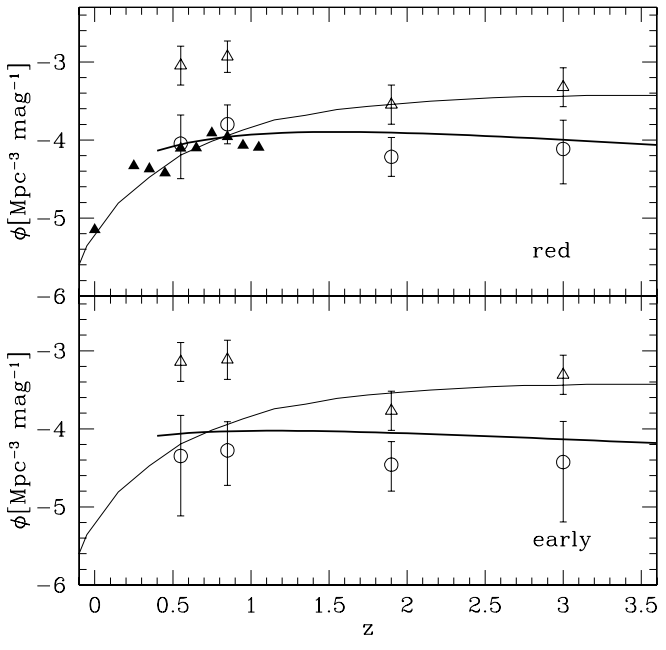

FIG. 12.—Density evolution as a function of redshift for red/early-type objects separated using the S0 evolutionary tracks. Circles represent galaxies in the range $-23 < M_B < -22$ and in the same redshift intervals used to compute the LFs. Open triangles represent galaxies in the range $-21.5 < M_B < -20.6$. Filled triangles are from the Schechter LFs of Bell et al. (2002). The thin continuous curve comes from the PLE model discussed in the text and computed at $M_B = -22.5$. The thick continuous curve comes from the integration of the best-fit LFs in the range $-23 < M_B < -22$. The upper panel shows the color-selected galaxies, while the lower panel shows galaxies selected according to their SSFR, as in Figs. 7 and 8.

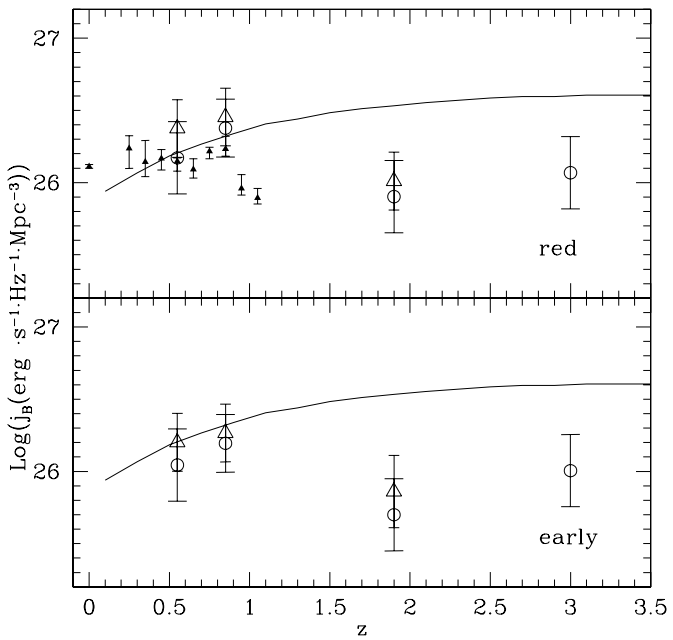

FIG. 13.—Luminosity density in the rest-frame *B* band of the red/early-type galaxies selected as in Fig. 12. Galaxies separated by their rest-frame $U-V$ color are shown in the upper panel, while those separated by their $\dot{m}_*/m_*$ are shown in the lower panel. The open circles represent the contribution from bright galaxies with $M_B < -20.6$, which are at the faintest limit of our sample at $z \sim 3$. Open triangles represent the contribution from galaxies with $M_B < -19.5$ for comparison with the Bell et al. (2002) data (*filled triangles*) at $z < 1$. The curve represents the passive evolution model shown in the previous figure for galaxies with $M_B < -20.6$.

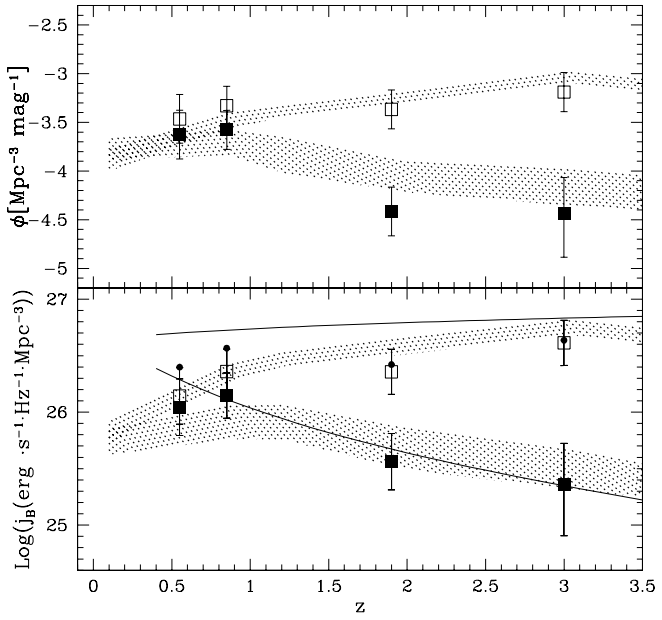

FIG. 14.—Number and *B*-band luminosity densities of early- (*filled squares*) and late-type (*open squares*) galaxies separated by their bimodal $\dot{m}_*/m_*$ distribution. Only galaxies with $-24 < M_B < -20.6$ are considered. The *B*-band luminosity density of the bright early- plus late-type galaxies is shown as small filled circles in the lower panel. The continuous lines represent the "total" luminosity densities of the early and late-type galaxies obtained after integration of the best-fit LFs down to $M_B = -15.8$. The shaded regions represent the uncertainties of the predictions of our CDM model due to the spread in the $\dot{m}_*/m_*$ threshold adopted and the dust extinction curves (SMCs, Milky Way, and Calzetti) affecting the luminosity cut.

this redshift interval could require more complex parametric evolutions. In any case, while at $z < 1$ both populations give a comparable contribution to the total *B*-band luminosity density, at $z > 1$ the contribution of the red population is much lower. This results in a global luminosity density of galaxies with $M_B < -20.6$ almost constant with redshift in the same *z*-interval.

Since we have seen in Paper I that there is a strong correlation between the observed rest-frame blue luminosity and the star formation rate for the blue/late population, this implies that the star formation activity in star-forming galaxies increases slightly or keeps constant up to $z = 3$. On the contrary, the number of galaxies with low specific star formation rates $\log \dot{m}_*/m_* < -10.5$, which are representative of an old stellar population with high formation redshift $z > 3$, decreases quickly.

This behavior is in qualitative agreement with that expected from a hierarchical clustering scenario in which galaxies with low specific star formation are located in the rare peaks of high dark matter density at high redshifts. However, a detailed quantitative comparison of specific CDM models is required to understand which physical mechanisms govern the early evolution of galaxies. A first attempt is done in the next section.

6.2. *Predictions by CDM Models*

To understand how the above results fit into current hierarchical models of galaxy formation, we used our semianalytic model (SAM). Starting from primordial density perturbations in a ΛCDM universe, the model describes the collapse and merging histories of the DM haloes that originate from such perturbations. In previous papers (see, e.g., Menci et al. 2002) we have described our model in detail; it includes the dynamical friction and the binary aggregations, determining the fate of clumps included into larger DM haloes along the hierarchy of mergers. The baryonic processes (gas cooling, star formation, and supernova feedback) are linked to the dynamical history of the galaxies through the simple recipes adopted by current SAMs (Kauffmann et al. 1993; Cole et al. 1994; Somerville & Primack 1999; Poli et al. 1999; Wu et al. 2000; Cole et al. 2000).

In this paper we are interested in the whole distribution of colors for any given galactic mass and redshift. In turn, such distribution depends on the different galaxy merging histories leading to a given galactic mass. Thus, we updated our model to describe the *scatter* in the galactic properties (SFR, colors) due to different merging histories, which could not be treated with our earlier model (Menci et al. 2004). To that aim, we built a Monte Carlo version of our SAM, in which different histories are generated by extracting the merging probability according to the prescription of the extended Press-Schechter theory; the corresponding galactic mass function is computed from such numerical realization (at variance with the method used in Menci et al. 2002; 2004).

The properties of the gas and stars contained in the galactic DM clumps are computed as in Menci et al. (2004). The only differences are that now (1) stars are allowed to form with rate $\dot{m}_* = m_c/t_*$, with the star formation timescale t_* assumed to be proportional to the disk dynamical time $t_* = q\, r_d/v_d$ through the proportionality constant q, which is left as a free parameter; (2) the mass Δm_h returned from the cool to the hot phase is estimated to be $\Delta m_h = E_{\rm SN}/v_{\rm esc}^2$, where $E_{\rm SN} = 10^{51}$ ergs $\epsilon_0 \eta_0 \Delta m_*$ is computed from the mass Δm_* of stars formed assuming $\eta_0 \approx (3-5) \times 10^{-3}$ for the number of SNe per unit solar mass (depending on the assumed IMF); and (3) assuming $\epsilon_0 = 0.01-0.5$ for the efficiency of the energy transfer to the interstellar medium whose value is highly uncertain (see, e.g., Kauffmann et al. 1993; Somerville & Primack 1999). The model free parameters q and ϵ_0 are chosen in order to match the local *B*-band galaxy and the Tully-Fisher relation. We adopt a Salpeter IMF with a standard value $\epsilon_0 = 0.1$

At each merging event, the masses of the different baryonic phases are replenished by those in the merging partner; the further increments Δm_c, Δm_*, and Δm_h from cooling, star formation, and feedback are recomputed on iterating the procedure described above. In our Monte Carlo code we adopt the description of starbursts triggered by major/minor merging and galactic fly-by following the formulation in Menci et al. (2004).

At higher *z*, the model results match the observed *K*-band LF (Pozzetti et al. 2003) up to $z = 1.5$ and the UV LFs measured for Lyman-break galaxies at $z = 3-4$. The global star formation history predicted by the model is consistent with that observed up to redshift $z \approx 4-5$ (Fontana et al. 2003a; Giavalisco et al. 2004), and the predicted stellar mass functions fit the observed ones (Cole et al. 2001; Fontana et al. 2004) up to $z = 1.5$. Given the above agreement concerning the *average* properties of the galaxy population (i.e., the properties averaged over all the merging histories), the comparison of the SAM results with the LF of populations with different $\dot{m}_*/m_*$ constitutes a higher order probe of the formation history of galaxies, which allows us to also test the properties of populations with particular merging histories.

The predictions by our CDM model concerning number and luminosity densities are shown in Figure 14 for both populations (late and early) adopting the same empirical separation derived from the observed bimodal distribution. Indeed, the model shows a clear bimodal distribution pointing toward the

same color dichotomy found in the data. A detailed analysis of the model bimodal distribution will be presented in a subsequent paper. We note that since the red/early LFs at all redshifts are rather flat around $M_B \sim -20.5$, the comparison of the model predictions depends only weakly on the magnitude cut.

We have to keep in mind that the threshold in the $\dot{m}_*/m_*$ adopted to separate the two populations could be subject to systematic underestimates, especially concerning the stellar mass derived from the observed SEDs, as discussed in § 3. In particular, the "maximal age approach" yields stellar masses a factor of 2 larger (Fontana et al. 2004); thus, we conservatively adopt in the predicted distribution of $\log(\dot{m}_*/m_*)$ a spread ranging from the default threshold (-10.5, corresponding to the best-fit observed stellar mass estimate) up to an offset of 0.3. The assumed uncertainty in the threshold propagates to the model predictions concerning the number/luminosity densities, as represented by the shaded regions in Figure 14. In principle, an additional source of uncertainty is represented by modeling the dust extinction curve, which affects the derived SFR. However, for galaxies with $\dot{m}_*/m_*$ around the threshold value, the low amount of dust makes this uncertainty much lower than that related to the stellar mass.

Figure 14 shows a broad agreement between the observed and the predicted evolutions of the early- and late-type galaxies with $M_B < -20.6$. In particular, a decrease in the number/luminosity density of red/early galaxies by a factor of 3–4 with respect to the local value is predicted at $2 < z < 3$. Thus, finding red objects at high-z is not inconsistent, by itself, with hierarchical clustering scenarios. This is because the clumps that end up in massive, bright objects are predicted to have older stellar populations (and hence redder colors) on average, since they formed in rare, high-density (biased) regions at high redshifts. The higher densities present in these regions have provided enhanced star formation, rapidly exhausting the cold gas reservoir.

Thus, at the level of detail of the present SAMs, it is remarkable that a clear distinction between the evolutionary trends of the two populations is predicted by this class of models. A detailed study of the link between the different merging histories leading to the two different populations will be presented in a future paper.

A similar behavior is also expected in the hydrodynamic simulations by Nagamine et al. (2004), in which an appreciable number of massive (and hence mostly red) galaxies is predicted at $z \sim 3$.

In this comparison we should keep in mind, however, that several uncertainties also affect the data points. Field-to-field variance due to clustering could affect, in particular, the number of early-type galaxies observed at high redshifts in small fields. Moreover, the average fraction of early-type galaxies in the red population ($\sim$60%; see the last column of Table 2) is statistical in nature and based on the fitting of the SED distribution with the spectral synthesis models. However, unless this fraction offers much different results after detailed spectroscopic analysis of the red sample, the conclusion is that the present CDM models are able to predict the presence of a number of early-type galaxies up to $z = 3.5$, which is comparable to that observed.

7. SUMMARY

We have used a composite sample of I-, H-, and K-selected galaxies to derive the evolution of the B-band LF of galaxies separated by their rest-frame $U - V$ color or specific (i.e., per unit mass) star formation rate up to $z \sim 3$. The observed color or SSFR distributions appear bimodal up to $z \sim 2.5-3$, extending to high redshift the same behavior recently found at low and intermediate redshifts. In particular, the bimodality in the SSFR distribution depends weakly on the luminosity of the sources in the luminosity interval probed by the present sample and evolves little from $z \sim 0.5$ to 3.

We adopted two different criteria to classify the galaxies and study the evolution of the LF of the red/early and blue/late populations. Focusing on the evolution of the early galaxies, we first adopted the null hypothesis that bright red/early galaxies are mainly affected by substantial passive luminosity evolution. For this reason we have adopted the color/SSFR passive evolutionary tracks of a galaxy whose local color is similar to that of a typical S0 galaxy to separate the two populations as a function of redshift. The resulting qualitative behavior of the LF does not depend significantly on the parameter used for the selection, $U - V$ color, or SSFR, implying that the contamination of dusty star-forming galaxies in the red sample, although substantial in number, does not modify appreciably the global evolutionary properties of the population.

Adopting a Schechter shape, the LF slope of the blue/late population is ~ -1.4 up to $z \sim 2.5$, while that of the red/early population is flatter (~ -0.5), extending to higher redshifts the similar difference found at $z < 1$. The evolution of the LF of blue and red galaxies is described in parametric form by the presence of both luminosity and density evolution. The evolution of the blue population is mainly driven by luminosity evolution, while appreciable density evolution characterizes the red/early population. In particular, a decline by a factor of the order of 5 results from $z \sim 0.4$ to 3. This implies that the red/early population as a whole cannot be described by simple pure luminosity evolution models; however, major dynamical events could act at high redshifts.

For this reason we also adopted an empirical criterion to separate the two galaxy populations, based on the presence of a minimum in the bimodal observed color/SSFR distribution in each redshift interval. The evolutionary difference between the two populations is even more marked in this case, with a density decline of the early population by about 1 order of magnitude from $z \sim 0.4$ to 3 at $M_B \sim -21,\ -21.5$.

The amount of mixed luminosity-density evolution depends on the assumed parameterization of the LF. We have also directly evaluated the volume and luminosity density of galaxies as a function of redshift in given intervals of absolute magnitudes. We have adopted both selection criteria to separate the two galaxy populations. Assuming the "S0 passive evolutionary cut," we have found that while the faint red/early population decreases slightly with redshift, the brightest fraction with $M_B < -22$ is consistent with being constant with redshift up to $z \sim 3$. A simple PLE model, in which galaxies are formed at high redshifts, overestimates the bright fraction at $z \sim 3$ by a factor of the order of 5.

Adopting the empirical criterion, we have found that the volume and luminosity densities of the early and late populations having $M_B < -20.6$, which is the faint limit in the highest redshift bin, appear to have a bifurcation at $z > 1$. In particular, while star-forming galaxies increase slightly or keep constant their luminosity density, early galaxies decrease in their luminosity density by a factor of $\sim$5–6, from $z \sim 0.4$ to $z \sim 2.5-3$.

A comparison of our latest version of hierarchical CDM models shows that a clear distinction between the different evolutionary histories of the early- and late-type galaxies is

predicted, in good agreement with the observations in which the contribution in the luminosity density of the early population is 10–20 times below that of the late population at $z \sim 3$. It is clear, however, that a more detailed comparison requires larger surveys to reduce the effects of the field-to-field variance and at the same time a better description in the CDM models of the physical mechanisms governing the different cosmic histories of the two populations.

We thank the anonymous referee for helpful comments. We also thank A. Cimatti for the use of the K20 survey data.

REFERENCES

Avni, Y., & Bahcall, J. N. 1980, ApJ, 235, 694
Baldry, I. K., Glazebrook, K., Brinkmann, J., Ivezić, Z., Lupton, R. H., Nichol, R. C., & Szalay, A. S. 2004, ApJ, 600, 681
Bell, E. F., et al. 2002, ApJ, 608, 752
Bertin, E., & Arnouts, S. 1996, A&AS, 117, 393
Blanton, M. R., et al. 2001, AJ, 121, 2358
———. 2003, ApJ, 594, 186
Bouwens, R. J., Illingworth, G. D., Blakeslee, J. P., Broadhurst, T. J., & Franx, M. 2004, ApJ, 611, L1
Brinchmann, J., Charlot, S., White, S. D. M., Tremonti, C., Kauffmann G., Heckman, T., & Brinkmann J. 2004, MNRAS, 351, 1151
Brinchmann, J., & Ellis, R. S. 2000, ApJ, 536, L77
Bruzual, G., & Charlot, S. 2003, MNRAS, 344, 1000
Casertano, S., et al. 2000, AJ, 120, 2747
Cimatti, A., et al. 2002, A&A, 392, 395
———. 2004, Nature, 430, 184
Cohen, J. G., Hogg, D. W., Blandford, R., Cowie, L. L., Hu, E., Songaila, A., Shopbell, P., & Richberg, K. 2000, ApJ, 538, 29
Cole, S., Aragon-Salamanca, A., Frenk, C. S., Navarro, J. F., & Zepf, S. E. 1994, MNRAS, 271, 781
Cole, S., Lacey, C., Baugh, C. M., & Frenk, C. S. 2000, MNRAS, 319, 168
Cole, S., et al. 2001, MNRAS, 326, 255
Dickinson, M., Papovich, C., Ferguson, H. C., & Budavari, T. 2003, ApJ, 587, 25
Ellis, R. S. 1997, ARA&A, 35, 389
Fontana, A., D'Odorico, S., Poli, F., Giallongo, E., Arnouts, A., Cristiani, S., Moorwood, A., & Saracco, P. 2000, AJ, 120, 2206
Fontana, A., Poli, F., Menci, N., Nonino, M., Giallongo, E., Cristiani, S., & D'Odorico, S. 2003a ApJ, 587, 544
Fontana, A., et al. 2003b, ApJ, 594, L3
———. 2004, A&A, 424, 23
Gehrels, N. 1986, ApJ, 303, 336
Giacconi, R., et al. 2001, ApJ, 551, 624
Giavalisco, M., et al. 2004, ApJ, 600, L103
Glazebrook, K., et al. 2004, Nature, 430, 181
Guzman, R., et al. 1997, ApJ, 489, 559
Heyl, J., Colless, M., Ellis, R. R., & Broadhurst, T. 1997, MNRAS, 285, 613
Hogg, D. W., et al. 2002, AJ, 124, 646
James, F., & Roos, M. 1995, MINUIT Function Minimization and Error Analysis, version 95.03 (CERN Program Libr. Long Writeup D506; Geneva: CERN)
Kauffmann, G., White, S. D. M., & Guiderdoni, B. 1993, MNRAS, 264, 201
Kuntschner, H., Smith, R. J., Colless, M., Davies, R. L., Kaldare, R., & Vazdekis, A. 2002, MNRAS, 337, 172
Labbé, I., et al. 2003, AJ, 125, 1107
Lilly, S., Tresse, L., Hammer, F., Crampton, D., & Le Fèvre, O. 1995, ApJ, 455, 108
Marshall, H. L., Tananbaum, H., Avni, Y., & Zamorani, G. 1983, ApJ, 269, 35
Menci, N., Cavaliere, A., Fontana, A., Giallongo, E., & Poli, F. 2002, ApJ, 575, 18
Menci, N., Cavaliere, A., Fontana, A., Giallongo, E., Poli, F., & Vittorini, V. 2004, ApJ, 604, 12
Nagamine, K., Cen, R., Hernquist, L., Ostriker, J. P., & Springel, V. 2004, ApJ, 610, 45
Norberg, P., et al. 2002, MNRAS, 336, 907
Papovich, C., Dickinson, M., & Ferguson, H. C. 2001, ApJ, 559, 620
Papovich, C., et al. 2004, ApJ, 600, L111
Poli, F., Giallongo, E., Menci, N., D'Odorico, S., & Fontana, A. 1999, ApJ, 527, 662
Poli, F., Menci, N., Giallongo, E., Fontana, A., Cristiani, S., & D'Odorico, S. 2001, ApJ, 551, L45 (erratum 554, L127)
Poli, F., et al. 2003, ApJ, 593, L1 (Paper I)
Pozzetti, L., et al. 2003, A&A, 402, 837
Rudnick, G., et al. 2003, ApJ, 599, 847
Sandage, A., Tamman, G. A., & Yahil, A. 1979, ApJ, 232, 352
Schweizer, F., & Seitzer, P. 1992, AJ, 104, 1039
Shapley, A. E., Steidel, C. C., Adelberger, K. L., Dickinson M., Giavalisco, M., & Pettini, M. 2001, ApJ, 562, 95
Somerville, R. S., & Primack, J. R. 1999, MNRAS, 310, 1087
Vanzella, E., et al. 2001, AJ, 122, 2190
———. 2004, A&A, submitted (astro-ph/0406591)
Wolf, C., Meisenheimer, K., Rix, H.-W., Borch, A., & Kleinheinrich, M. 2003, A&A, 401, 73
Wu, K. K. S., Fabian, A. C., & Nulsen, P. E. J. 2000, MNRAS, 318, 889